Modelling light distributions of homogeneous versus discrete absorbers in light irrdiated turbid media

Verkruijsse, W.; Lucassen, G.W.; de. Boer, J.F.; Smithies, D.J.; Nelson, J.S.; van Gemert, M.J.C.

DOI
10.1088/0031-9155/42/1/003

Publication date
1997

Published in
Physics in Medicine and Biology

Phys. Med. Biol. **42** (1997) 51–65. Printed in the UK PII: S0031-9155(97)73173-7

Modelling light distributions of homogeneous versus discrete absorbers in light irradiated turbid media

Wim Verkruysse†, Gerald W Lucassen†‡, Johannes F de Boer†, Derek J Smithies§, J Stuart Nelson§ and Martin J C van Gemert†‖

† Laser Centre, Academic Medical Centre at the University of Amsterdam, Meibergdreef 9, 1105 AZ Amsterdam, The Netherlands

§ Beckman Laser Institute and Medical Clinic, University of California, 1002 Health Sciences Rd East, Irvine, CA 92715, USA

Received 25 March 1996

Abstract. Laser treatment of port wine stains has often been modelled assuming that blood is distributed homogeneously over the dermal volume, instead of enclosed within discrete vessels. The purpose of this paper is to analyse the consequences of this assumption. Due to strong light absorption by blood, fluence rate near the centre of the vessel is much lower than at the periphery. Red blood cells near the centre of the vessel therefore absorb less light than those at the periphery. Effectively, when distributed *homogeneously* over the dermis, fewer red blood cells would produce the same absorption as the actual number of red blood cells distributed in discrete vessels. We quantified this effect by defining a correction factor for the effective absorbing blood volume of a single vessel. For a dermis with multiple vessels, we used this factor to define an *effective* homogeneous blood concentration. This was used in Monte Carlo computations of the fluence rate in a homogeneous skin model, and compared with fluence rate distributions using discrete blood vessels with equal dermal blood concentration. For realistic values of skin parameters the homogeneous model with corrected blood concentration accurately represents fluence rates in the model with discrete blood vessels. In conclusion, the correction procedure simplifies the calculation of fluence rate distributions in turbid media with discrete absorbers. This will allow future Monte Carlo computations of, for example, colour perception and optimization of vascular damage by laser treatment of port wine stain models with realistic vessel anatomy.

1. Introduction

Laser treatment of port wine stain (PWS) is an example of a medical application where light dosimetry is important for successful therapeutic results. The light fluence rate distribution in laser irradiated PWS skin tissue has often been calculated assuming a homogeneous distribution of blood (Pickering and van Gemert 1991, Verkruysse *et al* 1993, Kienle and Hibst 1995, Svaasand *et al* 1995). However, in PWS skin, blood is enclosed in discrete vessels rather than homogeneously distributed over the entire dermal volume. Unfortunately, as we will show, the assumption of a homogeneous distribution of blood can strongly overestimate attenuation of the fluence rate with dermal depth.

The assumption of a homogeneous distribution of absorbers has two computational advantages. First, if certain criteria are met (Star 1995), fluence rates can be calculated

‡ Present address: Philips Research Laboratories, Eindhoven, The Netherlands.

‖ Author to whom correspondence should be addressed (e-mail: m.j.vangemert@amc.uva.nl).

0031-9155/97/010051+15$19.50

very quickly using diffusion theory. Second, if the criteria for diffusion theory are not met, Monte Carlo computations are much faster for a homogeneous distribution as opposed to discrete absorbing structures (Smithies and Butler 1995, Keijzer *et al* 1989).

We present an analytical method which quantifies the difference in skin fluence rate between a homogeneous distribution and a discrete distribution of blood within vessels. The difference between the fluence rate distributions results from strong light attenuation within the vessel, producing a much smaller fluence rate near the centre than at the periphery. This implies that red blood cells located in the centre of the vessel contribute less to the total absorption of light than do those at the periphery. In contrast, assuming a homogeneous distribution of blood in the dermis, all red blood cells at a certain depth contribute equally to light absorption.

We quantify this effect by calculating the cross-sectional average fluence rate of a single blood vessel, as this is a measure for the fractional blood volume which absorbs the same amount of light as when distributed homogeneously over the dermis. If multiple vessels are represented by a homogeneous distribution of their blood content over the dermis, similar fluence rate distributions may be expected, provided the dermal blood concentration is corrected for the effective absorbing blood volume of each vessel. The aim of this paper is to show that a model with a homogeneously distributed *effective* dermal blood concentration provides fluence rate distributions similar to those obtained from a model with blood in discrete vessels.

2. Method

We calculate the cross-sectional average fluence rate Φ_{average} in a single blood vessel. Since absorption is proportional to the fluence rate, the average fluence rate is a measure for the total amount of light absorbed by the blood volume V of the whole vessel. By taking the ratio of the cross-sectional average fluence rate and the fluence rate Φ_0 outside the vessel, a correction factor C (with $0 < C < 1$) is obtained which is used to define the *effective blood volume* (the product of C and V) of the vessel which takes part in light absorption.

Thus the total absorption of light by the volume V in a vessel is

$$\mu_{\text{a,bl}}\,\Phi_{\text{average}}\;V = \mu_{\text{a,bl}}\,\Phi_0\,\frac{\Phi_{\text{average}}}{\Phi_0}\;V = \mu_{\text{a,bl}}\,\Phi_0\;C\;V \tag{1}$$

where $\mu_{\text{a,bl}}$ is the absorption coefficient of blood.

In this section, we first derive the correction factor for a single blood vessel, irradiated with diffuse or collimated light. Second, we will show how the results can be used to assess the average bulk optical properties of a dermis containing discrete vessels.

2.1. Derivation of the correction factor

2.1.1. Diffuse irradiation. We derive an expression for the fluence rate $\Phi(r)$ at a point O in the cross section of a horizontal vessel at a distance r from the centre C_{vessel} (figure 1). This expression is used to calculate the average fluence rate over the vessel cross-section.

In figure 1 we show a cylinder with radius R, representing a horizontal blood vessel in a three-dimensional Cartesian coordinate system. The origin of the Cartesian system coincides with point O which is at distance r from the vessel centre A. The cylinder surface is defined by

$$\begin{aligned} (y+r)^2 + x^2 &= R^2 \\ z &= z. \end{aligned} \tag{2}$$

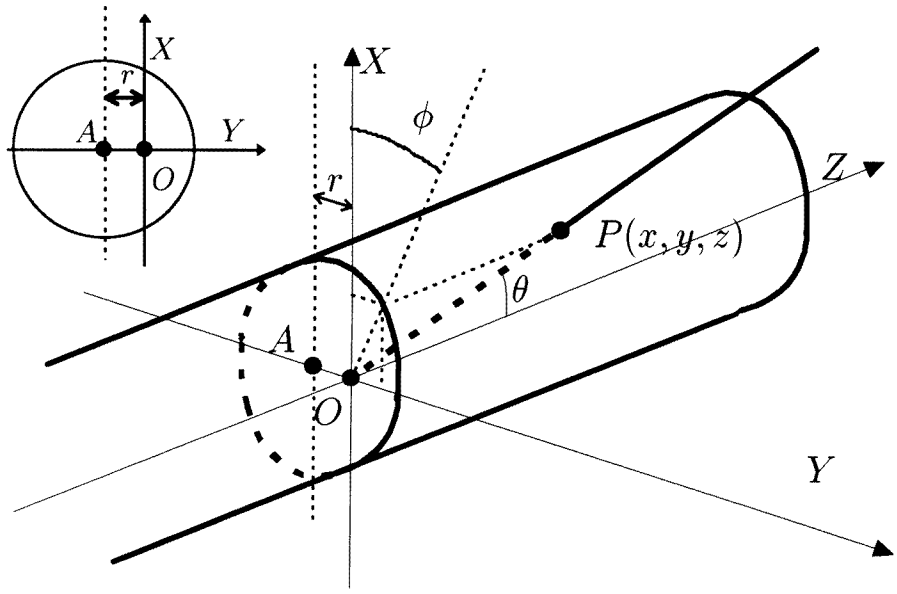

Figure 1. A horizontal cylinder representing a blood vessel. The straight thick broken line indicates the distance $\rho(r, \phi, \theta)$ over which the light beam, entering the vessel at point P, is attenuated before it contributes to the fluence rate in the origin O. A is the centre of the vessel, at distance r from the origin. The insert shows the position of the vessel with respect to the XY-plane.

Consider a light beam travelling towards point O which enters the vessel at point $P(x, y, z)$. The distance between P and O is ρ. For the subsequent calculations, it is convenient to use spherical coordinates ρ, θ and ϕ as indicated in figure 1. In spherical coordinates, x, y and z are given by

$$\begin{aligned} x &= \rho \sin(\theta) \cos(\phi) \\ y &= \rho \sin(\theta) \sin(\phi) \\ z &= \rho \cos(\theta). \end{aligned} \tag{3}$$

Substitution of equations (3) into equation (2) yields an expression for the cylinder surface in spherical coordinates. Solving for ρ gives

$$\rho(r, \phi, \theta) = \frac{-r \sin(\phi) + \sqrt{(r \sin(\phi))^2 + R^2 - r^2}}{\sin(\theta)}. \tag{4}$$

We assume the radiance at the vessel surface to be equal to L_0 in all directions to simulate totally diffuse light. Since absorption dominates over scattering for the blood within the vessel, the radiance $L(0, \theta, \phi)$ at the origin is approximately the radiance L_0 at the cylinder surface, attenuated over distance $\rho(r, \theta, \phi)$ according to Beer's law

$$L(0, \theta, \phi) = L_0 \exp(-\mu_{\mathrm{a,bl}}\ \rho(r, \theta, \phi)). \tag{5}$$

As the vessel is diffusely irradiated, the fluence rate $\Phi(r)$ at point O can be found by integrating the radiance $L(0, \theta, \phi)$ over 4π steradians

$$\Phi(r) = \int_{4\pi} L_0 \exp(-\mu_{\mathrm{a,bl}}\ \rho(r, \theta, \phi))\, \mathrm{d}\Omega \tag{6}$$

where $d\Omega = \sin(\theta)\, d\phi\, d\theta$. This expression gives the total fluence rate $\Phi(r)$ at a distance r from the vessel centre which is surrounded by totally diffuse light of radiance L_0. The fluence rate Φ_0 outside the vessel is

$$\Phi_0 = \int_{4\pi} L_0 d\Omega = 4\pi L_0. \tag{7}$$

We define the correction factor, C_{diff}, for the effective absorbing blood volume of a vessel illuminated by diffuse light as the ratio of the average fluence rate over the cross section of the vessel and the fluence rate outside the vessel

$$C_{\text{diff}}(R, \mu_{\text{a,bl}}) = \frac{\Phi_{\text{average}}}{\Phi_0} = \frac{\dfrac{1}{\pi R^2}\displaystyle\int_0^R 2\pi r \Phi(r)\, dr}{4\pi L_0}. \tag{8}$$

2.1.2. Collimated irradiation. A similar method is used to calculate the correction factor for a blood vessel irradiated with collimated light using the expression derived by Kimel *et al* (1994). As for diffuse irradiation, the correction factor $C_{\text{coll}}(R, \mu_{\text{a,bl}})$ is the ratio of the average fluence rate in a vessel and the fluence rate at the top of the vessel, yielding

$$C_{\text{coll}}(R, \mu_{\text{a,bl}}) = \frac{\dfrac{1}{\mu_{\text{a,bl}}}\displaystyle\int_{-R}^{R} \left(1 - \exp(-2\mu_{\text{a,bl}}\sqrt{R^2 - x^2})\right) dx}{\pi R^2}. \tag{9}$$

Equations (6), (8) and (9) were evaluated numerically. In appendices A and B we show that the correction factors $C_{\text{diff}}(R, \mu_{\text{a,bl}})$ and $C_{\text{coll}}(R, \mu_{\text{a,bl}})$ depend only on the product of R and $\mu_{\text{a,bl}}$ rather than on R and $\mu_{\text{a,bl}}$ individually. Therefore we can write $C_{\text{diff}}(R\,\mu_{\text{a,bl}})$ and $C_{\text{coll}}(R\,\mu_{\text{a,bl}})$ respectively.

2.2. Skin model

The skin model used in this paper consists of a dermis, with blood either distributed homogeneously (van Gemert *et al* 1986) or enclosed in discrete horizontal vessels of equal diameter. For simplicity, an epidermis was not incorporated because we wanted to focus on the effect of absorbing dermal structures.

The dermal blood concentration used was either 1% or 4%. For discrete vessels, the diameter and space between the vessels were varied to give four skin geometries (see table 1). The shortest distance between two adjacent vessel centres (δ) and radius (R) of the vessels as indicated in figure 2, are given in table 1 for each geometry used. Also given is the parameter D which is the periodicity of the vessels in the skin model.

All combinations of the scattering coefficient of the dermis and the absorption coefficients of blood, given in table 2, are used in each of the four skin geometries. The other optical properties used were: $\mu_{\text{a,der}} = 0.2\ \text{cm}^{-1}$, $\mu_{\text{s,bl}} = 500\ \text{cm}^{-1}$ and the anisotropy-values for blood and dermis were respectively $g_{\text{bl}} = 1$ and $g_{\text{der}} = 0.7$. These parameters are close to previously reported values (van Gemert *et al* 1991). We neglected scattering by blood ($g_{\text{bl}} = 1$).

2.3. Attenuation coefficients

The fluence rate in a homogeneous turbid medium tends to attenuate exponentially with tissue depth. We found that the average fluence rate in the skin model with discrete blood vessels also attenuates exponentially with depth. Therefore, we used exponential attenuation

Table 1. Characteristics of the four skin geometries used in the Monte Carlo calculations. The dermal blood concentration p, the vessel radius R, the shortest distance between two centres of neighbouring vessels δ, and the periodicity of the vessel distribution D are given (figure 2).

Geometry	p (%)	R (μm)	δ (μm)	D (μm)
1	4	32	284	401
2	1	32	567	802
3	1	64	1134	1604
4	1	8	142	201

Table 2. Values for the absorption coefficient of blood and scattering coefficient of the dermis used in each skin geometry. The other optical properties used were constant: dermal absorption coefficient $\mu_{a,der} = 0.2$ cm^{-1}, blood scattering coefficient $\mu_{s,bl} = 500$ cm^{-1} and the anisotropy values for blood and dermis $g_{bl} = 1$ respectively $g_{der} = 0.7$.

$\mu_{a,bl}$(cm^{-1})	$\mu_{s,der}$(cm^{-1})
60	200
125	400
250	600
500	-
1000	-
2000	-
4000	-

coefficients to compare the fluence rate distributions for discrete and homogeneous distributions of blood. In this subsection, we define the attenuation coefficients.

2.3.1. Discrete model. The Monte Carlo algorithm of Lucassen *et al* (1996), adapted from the code of Keijzer *et al* (1989), was used to calculate the fluence rate distribution in the discrete skin geometries. We simulated diffuse illumination since we wanted the light to be diffuse immediately under the surface. We neglected a refractive index change at the dermal surface and the spot size is assumed to be infinite Keijzer *et al* (1991) to prevent an influence on the average attenuation coefficient from these parameters. We also neglected a refractive index change at the blood vessel–dermis interface.

The grid defined in the Monte Carlo model and indicated (not to scale) in figure 2 consists of boxes with size of $D/50$ in the y-direction and $D/20$ in the x-direction, where D is the blood vessel periodicity.

To determine a value for the average fluence rate attenuation in the Monte Carlo model, we compared the fluence rate $\phi(x)$ in a grid box at (x, y) with $\phi(x - D)$ in a grid-box with the same lateral position y but at depth $x - D$. The attenuation coefficient of the light fluence rate for these two boxes is given by

$$\mu_{\text{discr}}(x, y) = \frac{1}{D} \ln\left(\frac{\phi(x - D, y)}{\phi(x, y)}\right). \tag{10}$$

We determined (10) for all box pairs in the grid, varying the x and y positions. We define the average attenuation in the discrete model as

$$\mu_{\text{discr}} = \frac{1}{N} \sum_{(i,j)}^{N} \frac{1}{D} \ln\left(\frac{\phi(x_i - D, y_j)}{\phi(x_i, y_j)}\right) \tag{11}$$

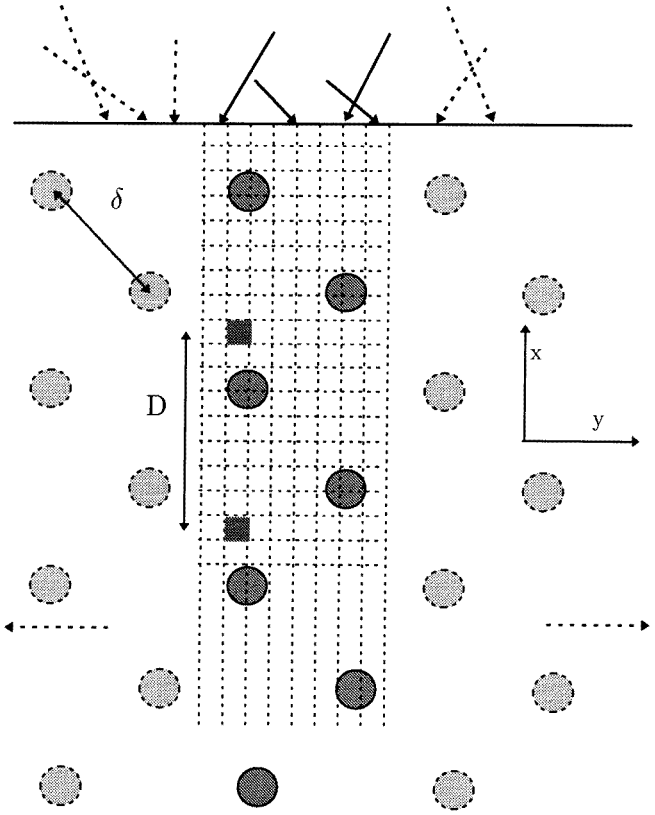

Figure 2. The distribution of the discrete vessels in the skin model. The Monte Carlo algorithm is adapted such that the distribution of the vessels shown is extended infinitely to the left and the right (dashed lines). We indicate an example of a set of two boxes (dark squares) from which the attenuation of the fluence rate was calculated. This figure indicates the relative position of the vessels and is not to scale.

where N is the number of box pairs in the grid excluding the number of pairs for which the attenuation was observed to be influenced by boundary conditions. N was about 2500 using about 50 box pairs in the x-direction and 50 in the y-direction.

2.3.2. Homogeneous model. For a homogeneous distribution, the dermal and blood optical properties are usually combined to bulk optical properties according to

$$\begin{aligned} \mu_{\mathrm{a,mix}} &= (p\,\mu_{\mathrm{a,bl}} + (100-p)\mu_{\mathrm{a,der}})/100 \\ \mu_{\mathrm{s,mix}} &= (p\,\mu_{\mathrm{s,bl}} + (100-p)\mu_{\mathrm{s,der}})/100 \\ g_{\mathrm{mix}} &= \frac{p\ \mu_{\mathrm{s,bl}}\ g_{\mathrm{bl}} + (100-p)\,\mu_{\mathrm{s,der}}\ g_{\mathrm{der}}}{p\ \mu_{\mathrm{s,bl}} + (100-p)\,\mu_{\mathrm{s,der}}} \end{aligned} \tag{12}$$

where p is the volumetric dermal blood fraction in %. For the standard relationship of the g-value of the mixture, see Graaff *et al* (1992). The fluence rate attenuation coefficient in a homogeneous mixture is, according to diffusion theory

$$\mu_{\mathrm{homog}} = \sqrt{3\mu_{\mathrm{a,mix}}\,(\mu_{\mathrm{a,mix}} + \mu_{\mathrm{s,mix}}(1-g_{\mathrm{mix}}))} \tag{13}$$

with the optical properties of the mixture given in equations (12).

We apply the correction factor, equation (8) or (9), to obtain a new set of bulk optical properties of the dermis. In the new set, the dermal blood concentration is corrected for the limited light penetration in a vessel. The fractional skin volume containing blood is multiplied by the correction factor giving the *effective* dermal blood concentration. The remaining skin volume fraction which does not contain blood vessels is obviously unchanged. So equations (12) become

$$\begin{aligned} \mu_{\mathrm{a,mix,eff}} &= (C\ p\ \mu_{\mathrm{a,bl}} + (100-p)\mu_{\mathrm{a,der}})/100 \\ \mu_{\mathrm{s,mix,eff}} &= (C\ p\ \mu_{\mathrm{s,bl}} + (100-p)\mu_{\mathrm{s,der}})/100 \\ g_{\mathrm{mix,eff}} &= \frac{C\ p\ \mu_{\mathrm{s,bl}}\ g_{\mathrm{bl}} + (100-p)\,\mu_{\mathrm{s,der}}\ g_{\mathrm{der}}}{C\ p\ \mu_{\mathrm{s,bl}} + (100-p)\,\mu_{\mathrm{s,der}}} \end{aligned} \tag{14}$$

where C is either $C_{\mathrm{diff}}(R, \mu_{\mathrm{a,bl}})$ or $C_{\mathrm{coll}}(R, \mu_{\mathrm{a,bl}})$, equation (8) or (9). The new attenuation coefficient $\mu_{\mathrm{homog,eff}}$ follows from (13)

$$\mu_{\mathrm{homog,eff}} = \sqrt{3\mu_{\mathrm{a,mix,eff}}\,(\mu_{\mathrm{a,mix,eff}} + \mu_{\mathrm{s,mix,eff}}(1-g_{\mathrm{mix,eff}}))}. \tag{15}$$

2.4. The fluence rate inside a vessel

We used a Monte Carlo model to calculate the fluence rate in and around a diffusely irradiated vessel with a radius of 50 μm. We did this for two reasons; first, to test our expression for the fluence rate inside a vessel (equation (6)), and second, to investigate the influence of dermal scattering on the fluence rate in and around the vessel. To simulate an irradiance as diffuse as possible, photons were launched from two opposing surfaces of a cube (400 μm) with reflecting sides. The vessel was positioned in the centre of the cube, running parallel to the launching surfaces. The fluence rate was calculated between the two launching surfaces, cross-sectioning the vessel, and was normalized to the fluence rate at the boundary of the cube. The absorption coefficients of blood $\mu_{\mathrm{a,bl}}$ were 100 cm^{-1} and 250 cm^{-1}. Values for the dermal scattering coefficient are $\mu_{\mathrm{s,der}} = 200$ cm^{-1} and 600 cm^{-1}. The anisotropy factor g_{der} is 0.7. Scattering within the blood vessel was neglegted ($g_{\mathrm{bl}} = 1$).

3. Results

3.1. The fluence rate within vessels for diffuse irradiation

In appendix A, we show how equation (6) can be rewritten as a function of relative distance r/R and the product $R\ \mu_{\mathrm{a,bl}}$. We use the scaling properties of equation (6) to plot the numerical solution of this equation in figure 3, normalized to Φ_0. Two examples are shown with $R\ \mu_{\mathrm{a,bl}}$ values of 0.5 and 1.25. The fluence rates from the model have a discontinuity at the vessel wall. The normalized fluence rates outside the vessel are by definition equal to 1. The broken curves represent the fluence rate in a cross section through the vessel centre as determined from Monte Carlo calculations. For the lower dermal scattering coefficient ($\mu_{\mathrm{s,der}} = 200$ cm^{-1}), the two models give virtually identical results. For the higher dermal scattering coefficient ($\mu_{\mathrm{s,der}} = 600$ cm^{-1}), the results from the Monte Carlo calculations are slightly lower than those predicted by equation (6). Outside the vessel, the normalized fluence rate is less than 1 near the vessel and gradually becomes equal to 1 for larger relative distances from the vessel centre.

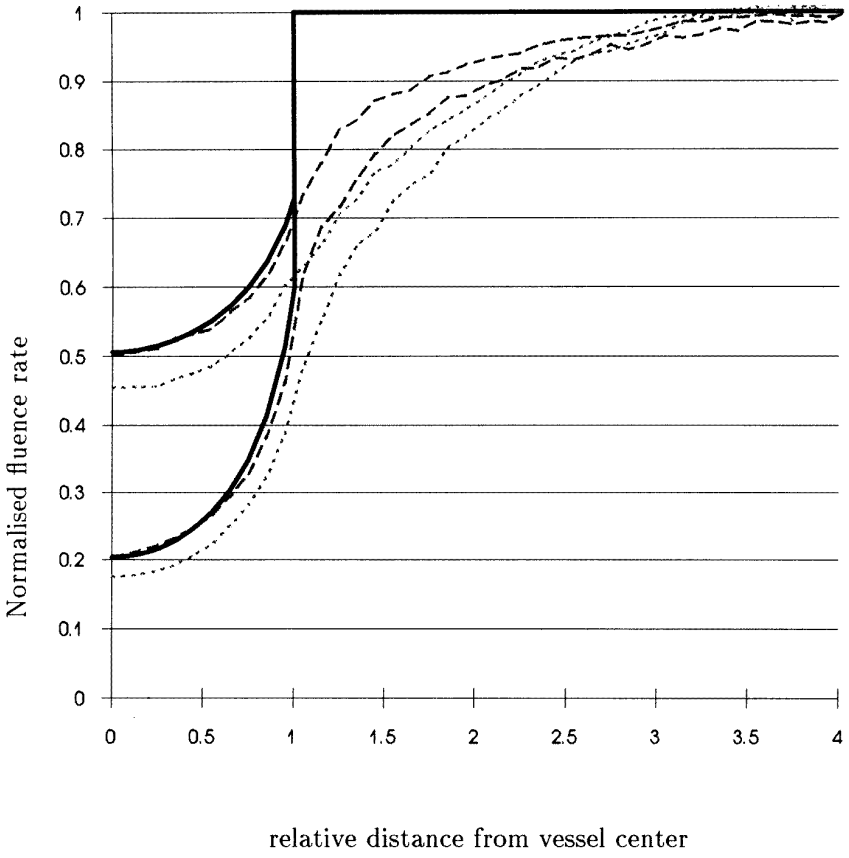

Figure 3. Fluence rate in and around a vessel as a function of the relative distance r/R from the vessel centre. The upper and lower set of curves is for $R\ \mu_{a,bl}$ = 0.5 and $R\ \mu_{a,bl}$ = 1.25 respectively. Full curves are the fluence rates obtained from equation (6) and the broken curves are results from Monte Carlo computations in which a vessel with radius $R = 50\ \mu$m was diffusely irradiated. The Monte Carlo computations are done for two values of the dermal scattering coefficients $\mu_{s,der} = 200\ cm^{-1}$ (– – –) and $\mu_{s,der} = 600\ cm^{-1}$ (- - - -). These fluence rates are normalized to the value at the boundary of the cube.

3.2. Homogeneous distribution of blood corrected for the effective blood volume

In figure 4 correction factors for the effective absorbing blood volume of a single blood vessel for both collimated and diffuse irradiation (equations (8) and (9)), are given as a function of the product of vessel radius R and blood absorption coefficient $\mu_{a,bl}$. The larger the product of vessel radius and blood absorption coefficient, the more important the correction factor. The effective absorbing blood volume of a vessel is slightly larger for collimated than for diffuse vessel irradiation.

In figure 5, fluence rate distributions in tissue as a function of depth are shown, calculated with the Monte Carlo program for vessel geometry 2 (table 1). Three cases are shown: first, for the discrete distribution of blood vessels; second, for an uncorrected homogeneous distribution of blood; and, third, for the homogeneous distribution with an effective blood concentration. In these cases, the dermal scattering coefficient is 400 cm^{-1}

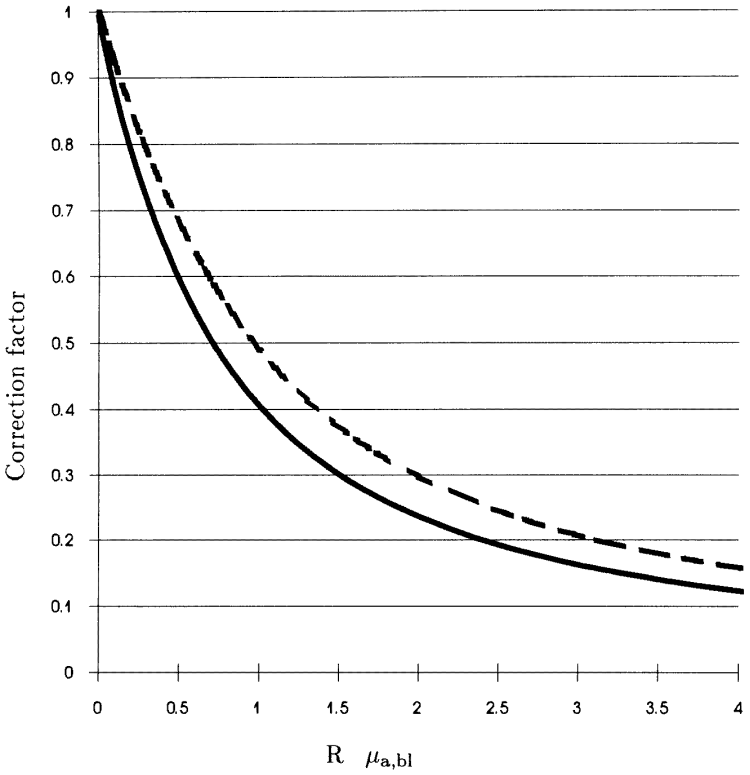

Figure 4. The correction factor $C_{diff}(R, \mu_{a,bl})$ for a diffuse (———) and $C_{coll}(R, \mu_{a,bl})$ for collimated irradiation (– – –) as a function of $R\ \mu_{a,bl}$.

and the blood absorption coefficient equals 500 cm^{-1}. The fluence rate for the uncorrected homogeneous distribution of blood is more attenuated than in the more realistic case of a discrete distribution of blood in vessels. There is excellent agreement between the fluence rates calculated in the corrected homogeneous model and those calculated in the discrete model with blood vessels.

3.3. The model for a range of optical parameters and geometries

In figures 6 and 7 we present the parameters μ_{homog} (13), $\mu_{homog,eff}$ (15) and μ_{discr} (11) as a function of $\mu_{a,bl}$. For the calculation of $\mu_{homog,eff}$, we used the correction factor for diffuse irradiation (8).

The difference between uncorrected attenuation coefficients μ_{homog} and corrected attenuation coefficients $\mu_{homog,eff}$ is larger for larger values of $\mu_{a,bl}$. The values for μ_{discr} for the discrete distribution of blood vessels and the curves for the corrected homogeneous distribution reach a maximum for large values of the blood absorption coefficient. In this range, only the outer edges of the vessels can absorb light because the centres are hardly reached by photons. Under such circumstances, the total light absorption by a vessel is virtually independent of $\mu_{a,bl}$.

For the case shown in figure 6, the most realistic case used to represent a PWS, values of $\mu_{homog,eff}$ correspond very well to the μ_{discr}. In figure 7, however, we see that the values of

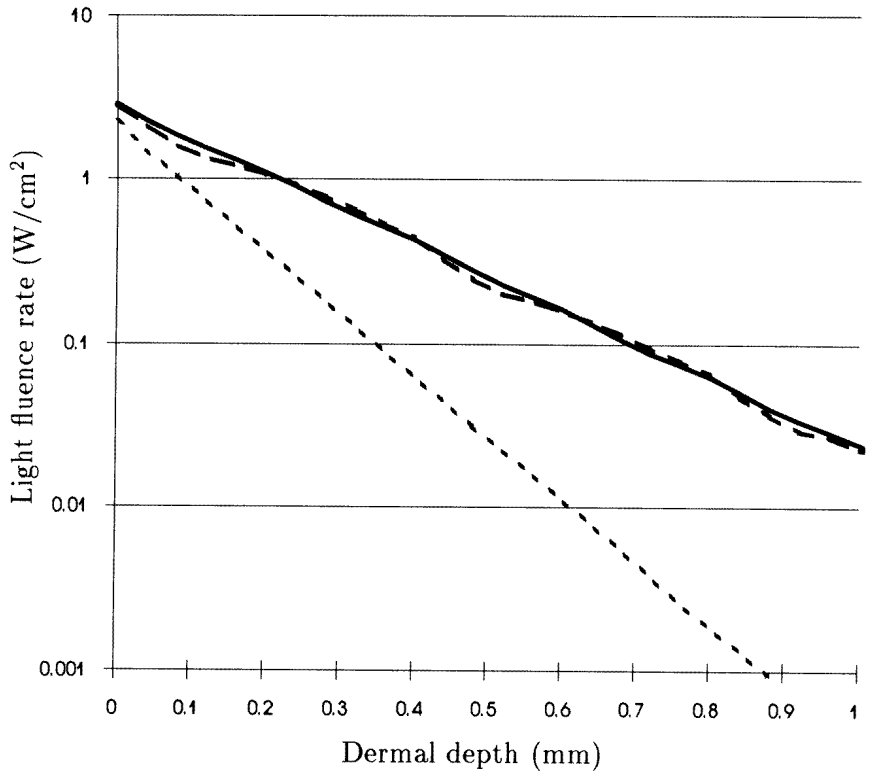

Figure 5. Fluence rate in tissue with 4% homogeneously distributed blood (- - - -) is more attenuated than the more realistic case where 4% of blood is distributed in discrete vessels with radius $R = 32$ μm (— —). Using the corrected dermal blood concentration in a homogeneous distribution, the fluence rate involved (——) provides an excellent representation for the fluence rate in the case of discrete blood vessels. The 'dips' in the fluence rate calculated for the discrete vessel distribution represent the influence of adjacent blood vessels.

$\mu_{\text{homog,eff}}$ are larger than the values of μ_{discr} for larger dermal scattering coefficients. Also, we found that the difference between μ_{discr} and $\mu_{\text{homog,eff}}$ is larger if two adjacent vessels are farther apart. In table 3 we give the ratio $\mu_{\text{discr}}/\mu_{\text{homog,eff}}$ for each of the four geometries and three dermal scattering coefficients. We have included in table 3 the ratio of the shortest distance between two adjacent vessel walls ($\delta - 2R$) and the reduced dermal scattering length (l'_s), which parameter is used in the discussion. The reduced dermal scattering length is the inverse value of $\mu_{\text{s,der}}(1 - g_{\text{der}})$ where $\mu_{\text{s,der}}$ is the dermal scattering coefficient and g_{der} the dermal anisotropy factor.

4. Discussion

4.1. Model relevance

In modelling laser treatment of PWS, using green (argon laser) or yellow light (copper-vapour, flashlamp pumped dye laser), a significant error can be made in the calculated light fluence rate distribution when the effect described in this paper is neglected. This was

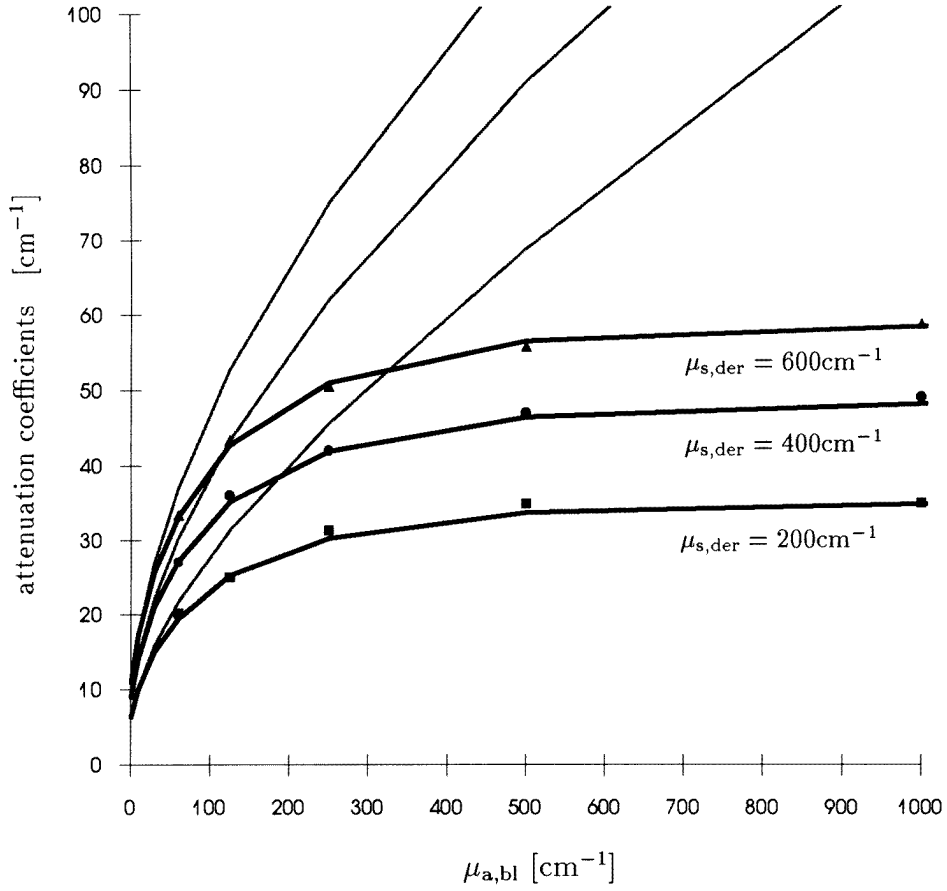

Figure 6. The effect of $\mu_{a,bl}$ on the derived bulk attenuation coefficients for the first vessel geometry in table 1 (vessel radius = 32 μm, dermal blood concentration = 4%); μ_{homog} (——) (equation (11)), $\mu_{homog,eff}$ (——) (equation (14)) and μ_{discr} (■, ●, ▲) (equation (13)) are drawn on the vertical axis. Three values of $\mu_{s,der}$ are used: 200 cm^{-1} (■), 400 cm^{-1} (●) and 600 cm^{-1} (▲).

done by Pickering and van Gemert (1991), Verkruysse *et al* (1993) and Kienle and Hibst (1995) who modelled the optimal wavelength for PWS laser treatment using proportional averaging of blood in the dermis for the bulk optical properties of a homogeneous skin layer. These models, and an animal study by Tan *et al* (1990) using pig skin, showed 585 nm to have a greater penetration depth than 577 nm. However, Smithies and Butler (1995) and Lucassen *et al* (1996) have shown with Monte Carlo modelling that in skin with a discrete distribution of blood vessels, the difference in penetration depths between 577 nm and 585 nm is much less than was expected from homogeneous models (Verkruysse *et al* (1993), Kienle and Hibst (1995)). The effect described in this paper completely explains the discrepancy, caused by the uncorrected homogeneous distribution of blood (figure 5). As an example, for the first vessel geometry (4% dermal blood, vessel radius 32μm) uncorrected attenuation coefficients for 577 nm and 585 nm are 55 cm^{-1} and 38 cm^{-1} respectively, whereas the corrected coefficients are 31 cm^{-1} and 27 cm^{-1} respectively (figure 6).

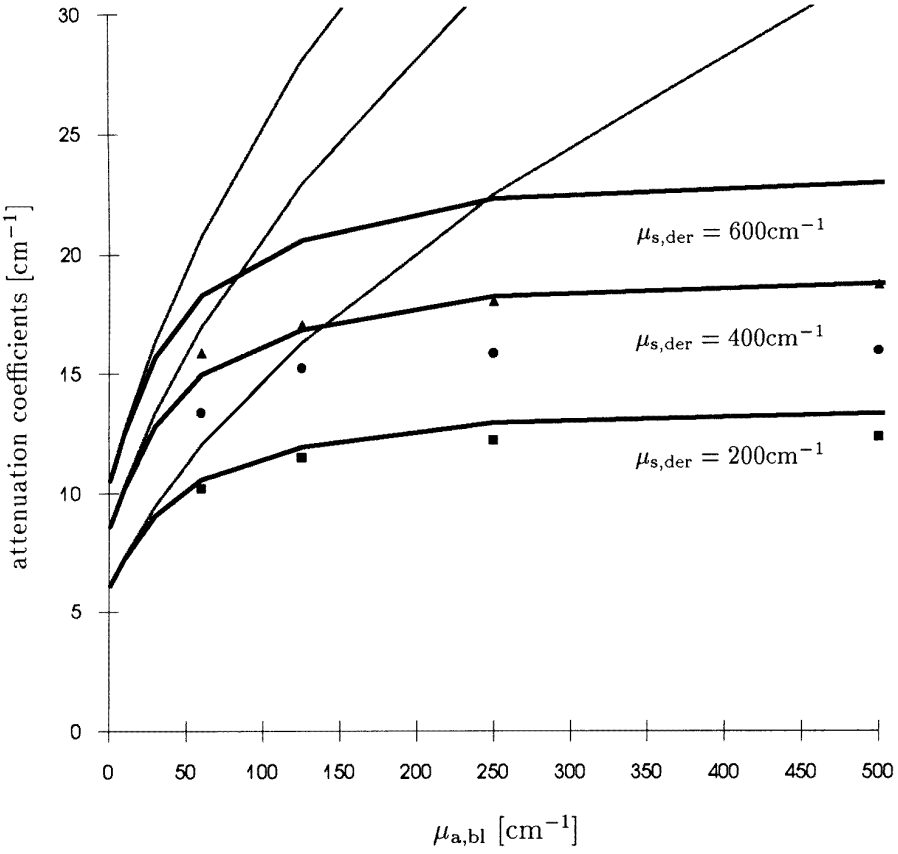

Figure 7. The effect of $\mu_{a,bl}$ on the derived bulk attenuation coefficients for the third vessel geometry in table 1 (vessel radius = 64 μm). The average attenuation coefficient μ_{discr} as found from the Monte Carlo calculations with discrete absorbers is lower than predicted by the model with corrected homogeneous blood concentration.

Not only in modelling laser irradiation of skin but in all other tissues with blood vessels it may be important to realize that a homogeneous distribution of blood can strongly overestimate the influence of light absorption by blood. This may be of particular importance in dosimetry for photodynamic therapy where both green (large absorption of light in blood) and red light (small absorption of light in blood) are used. Therefore, the correction for the effective concentration of blood differs significantly between these two wavelength regions. Another example of discrete absorbers in a turbid medium are melanosomes in the epidermis. From the density and volumes of the melanosomes, an underestimation of the absorption coefficient in a melanosome may be predicted when the average epidermal absorption is used without the correction formalism described in this paper.

4.2. Model validity

There can be large differences between the fluence rate distributions for the discrete distribution of blood vessels and the uncorrected homogeneous distribution of blood. When

Table 3. For each combination of skin geometry and dermal scattering coefficient, the ratio $\mu_{\text{discr}}/\mu_{\text{homog,eff}}$ is given in the left-hand columns. Values between parentheses represent the standard deviations. In the corresponding right-hand columns, ratios of the shortest distance between two adjacent vessel walls ($\delta - 2R$) and reduced dermal scattering lengths (l'_s) are given. There are five cases in which the value of μ_{discr} significantly deviates from $\mu_{\text{homog,eff}}$. For all these cases, the ratio $(\delta - 2R)/l'_s$ is equal to or greater than 6. For all other cases this ratio is less than 6.

Geometry	$\mu_{\text{s,der}} = 200\ \text{cm}^{-1}$		$\mu_{\text{s,der}} = 400\ \text{cm}^{-1}$		$\mu_{\text{s,der}} = 600\ \text{cm}^{-1}$	
	$\frac{\mu_{\text{discr}}}{\mu_{\text{homog,eff}}}$	$\frac{(\delta-2R)}{l'_s}$	$\frac{\mu_{\text{discr}}}{\mu_{\text{homog,eff}}}$	$\frac{(\delta-2R)}{l'_s}$	$\frac{\mu_{\text{discr}}}{\mu_{\text{homog,eff}}}$	$\frac{(\delta-2R)}{l'_s}$
1	1.02 (0.02)	1.3	1.02 (0.02)	2.6	1.01 (0.02)	4.0
2	0.99 (0.01)	3.0	0.97 (0.02)	6.0	0.92 (0.02)	9.1
3	0.95 (0.01)	6.0	0.88 (0.01)	12.1	0.84 (0.02)	18.1
4	0.97 (0.05)	0.8	0.99 (0.02)	1.5	1.02 (0.02)	2.3

the absorption length in blood (the inverse of $\mu_{\text{a,bl}}$) is large with respect to the vessel radius, the difference is negligible, as the fluence rate distribution within the vessel is almost uniform. If the absorption length in blood is small with respect to the vessel radius, the uncorrected homogeneous model is inadequate as a representation of discrete blood vessels. We have shown that the results from this model can be improved by including a correction factor for the effective blood volume in the skin. For most of the simulations reported in this paper, there is excellent agreement in the results between the discrete model and the corrected homogeneous model. However, in the cases of high dermal scattering, low blood content and large blood vessels (i.e. distance between adjacent vessels is large compared with the reduced dermal scattering length), we found μ_{discr} to be significantly lower than $\mu_{\text{homog,eff}}$. A possible explanation can be found by analysing figure 3. We hypothesize that high dermal scattering implies that photons incident on the blood vessel originate from a smaller dermal volume than in case of low dermal scattering. Consequently, in the case of high dermal scattering, the blood vessel disturbs the fluence rate around the vessel more than in the case of low scattering. This results in a lower average fluence rate inside the vessel than that calculated according to our expression (equation 6) and, consequently, a lower effective absorbing volume. The actual fluence rate, incident on the vessel is lower than the average fluence rate occurring at the dermal depth where the vessel is located. The relative difference between these fluence rates becomes larger for larger distances between the vessels (i.e. the dip in fluence rate around the vessel has a smaller influence on the average fluence rate). The dependence of this effect on the dermal scattering coefficient and distance between the vessels is expressed in the ratio of $(\delta - 2R)/l'_s$. As can be seen in table 3, the larger this ratio, the larger the deviation of μ_{discr} from $\mu_{\text{homog,eff}}$.

4.3. The correction factors used in a more realistic skin model

4.3.1. Various diameters. Dermal blood vessels in human skin have varying diameters, unlike the vessels used in this model. The correction factor in this paper, derived for a single vessel, enables us to use it for each vessel present in a skin model. For example, if, in a layer at a certain depth, the concentration of vessels with diameter R_1 is p_1 and the concentration of vessels with diameter R_2 is p_2, then the effective total blood concentration in this layer is: $C(R_1\,\mu_{\text{a,bl}})\ p_1 + C(R_2\,\mu_{\text{a,bl}})\ p_2$, where $C(R\,\mu_{\text{a,bl}})$ is either $C_{\text{diff}}(R, \mu_{\text{a,bl}})$ or $C_{\text{coll}}(R, \mu_{\text{a,bl}})$. Consequently, multiple layers can be defined in which an effective blood concentration is calculated for each individual layer.

4.3.2. Random vessel positions. The correction factor for the effective blood volume was derived for vessels that are positioned in a geometrically regular way. In reality, vessels are randomly positioned. This has implications for the correction factor; if two vessels are sufficiently close to each other as to influence the fluence rate distribution in that region, the effective local blood volume will be reduced.

4.3.3. Collimated and diffuse light. In practice, light is not totally diffuse because there is a collimated component, particularly in the upper tissue layers. Because there is a minimal difference between the correction factors for diffuse and collimated light, the correction factor for the diffuse case will be applicable in most cases of modelling laser irradiation of tissues containing discrete absorbers.

5. Conclusion

The use of a homogeneous distribution of blood to represent the influence of blood vessels on light distributions in skin tissue overestimates the influence of absorption of light by the blood if the absorption length $(1/\mu_{a,bl})$ is equal to or less than the vessel radius. A correction procedure has been defined whereby the concentration of homogeneously distributed blood is corrected for the non-uniform light absorption within each blood vessel. For realistic skin parameters, the homogeneous model with corrected blood concentration accurately represents the model with discrete blood vessels. If the reduced dermal scattering path length is much shorter than the distance between two adjacent vessels, the average attenuation of the fluence rate is significantly less than predicted by our correction procedure. The present method will allow future Monte Carlo computations of fluence rate distributions, colour perception and optimization of vascular damage in port wine stain models with realistic vessel anatomy.

Acknowledgments

This work was supported by the Dutch Technology Foundation (STW) grant AGN33.2964.

Appendix A. Scaling of the correction factor for diffuse irradiance

Substitution of $k = r/R$ with $0 \leqslant k \leqslant 1$, in equation (4) gives

$$\begin{aligned}\rho(k\,R, \phi, \theta) &= \frac{-k\,R\sin(\phi) + \sqrt{(k\,R\,\sin(\phi))^2 + R^2 - (k\,R)^2}}{\sin(\theta)} \\ &= R\,\frac{-k\sin(\phi) + \sqrt{(k\sin(\phi))^2 - k^2 + 1}}{\sin(\theta)} \\ &= R\;\rho(k, \phi, \theta). \end{aligned} \tag{16}$$

Equation (6) can therefore be expressed as a function of two parameters only: k and the product of R and $\mu_{a,bl}$

$$\begin{aligned}&= \int_{4\pi} L_0 \exp(-R\,\mu_{a,bl}\;\rho(k, \phi, \theta))\,\mathrm{d}\Omega \\ &= \Phi(k,\, R\;\mu_{a,bl}). \end{aligned} \tag{17}$$

Hence, using $\mathrm{d}r = R\,\mathrm{d}k$ in equation (8) gives

$$\begin{aligned} C_{\mathrm{diff}}(R, \mu_{\mathrm{a,bl}}) &= \frac{\int_0^1 2\pi R^2 k \int_{4\pi} L_0 \exp(-\mu_{\mathrm{a,bl}}\rho(k\,R, \phi, \theta))\,\mathrm{d}\Omega\,\mathrm{d}k}{4\pi^2 R^2 L_0} \\ &= \frac{\int_0^1 k\Phi(R\ \mu_{\mathrm{a,bl}}, k)\,\mathrm{d}k}{2\pi L_0} \\ &= C_{\mathrm{diff}}(R\,\mu_{\mathrm{a,bl}}). \end{aligned} \tag{18}$$

Appendix B. Scaling of the correction factor for collimated irradiance

For collimated irradiation we follow a similar procedure as in appendix A. The substitution $x = x'\,R$ and $\mathrm{d}x = \mathrm{d}x'\,R$ in equation (9) gives

$$\begin{aligned} C_{\mathrm{coll}}(R, \mu_{\mathrm{a,bl}}) &= \frac{1/\mu_{\mathrm{a,bl}} \int_{-1}^1 R\left(1 - \exp(-2\mu_{\mathrm{a,bl}}\sqrt{R^2 - (Rx')^2})\right)\,\mathrm{d}x'}{\pi R^2} \\ &= \frac{\int_{-1}^1 \left(1 - \exp(-2R\,\mu_{\mathrm{a,bl}}\sqrt{1 - x'^2})\right)\,\mathrm{d}x'}{\pi R\,\mu_{\mathrm{a,bl}}} \\ &= C_{\mathrm{coll}}(R\,\mu_{\mathrm{a,bl}}). \end{aligned} \tag{19}$$

References

Graaff R, Aarnoudse J G, Zijp J R, Sloot P M A, de Mul F F M, Greve J and Koelink M H 1992 Reduced light-scattering properties for mixtures of spherical particles: a simple approximation derived from mie calculations *Appl. Opt.* **31** 1370–6

Keijzer M, Jacques S L, Prahl S A and Welch A J 1989 Light distributions in artery tissue: Monte Carlo simulations for finite-diameter laser beams *Lasers Surgery Med.* **9** 148–54

Keijzer M, Pickering J W and van Gemert M J C 1991 Laser beam diameter for port wine stain treatment *Lasers Surgery Med.* **11** 601–5

Kienle A and Hibst R 1995 A new optical wavelength for treatment of port wine stains? *Phys. Med. Biol.* **40** 1559–76

Kimel S, Svaasand L O, Hammer-Wilson M, Schell M J, Milner T E, Nelson J S and Berns M W 1994 Differential vascular response to laser photothermolysis *J. Invest. Dermatol.* **103** 693–700

Lucassen G W, Verkruysee W, Keijzer M and van Gemert M J C 1996 Light distributions in a port wine stain skin model containing multiple cylindrical and curved blood vessels *Lasers Surgery Med.* at press

Pickering J W and van Gemert M J C 1991 585 nm for the laser treatment of port-wine stains: a possible mechanism (letter) *Lasers Surgery Med.* **11** 616–18

Smithies D J and Butler P H 1995 Modelling the distribution of laser light in port-wine stains with the Monte Carlo method *Phys. Med. Biol.* **40** 701–33

Star W 1995 Diffusion theory of light transport *Optical-Thermal Response of Laser-Irradiated Tissue* ed A J Welch and M J C van Gemert (New York: Plenum) pp 131–206

Svaasand L O, Norvang L T, Fiskerstrand E J, Stopps E K S, Berns M W and Nelson J S 1995 Tissue parameters determining the visual appearance of normal skin and port-wine stains *Lasers Med. Sci.* **10** 55–65

Tan O T, Morrison P and Kurban A K 1990 585 nm for the treatment of port-wine stains *Plastic Reconstruct. Surg.* **86** 1112–17

van Gemert M J C, Welch A J and Amin A 1986 Is there an optimal treatment for port wine stains? *Lasers Surgery Med.* **6** 76–83

van Gemert M J C, Welch A J, Miller I D and Tan O T 1991 Can physical modelling lead to an optimal laser treatment strategy for port-wine stains? *Laser Applications in Medicine and Biology* vol 5 ed M L Wolbarsht (New York: Plenum) pp 199–275

Verkruysse W, Pickering J W, Beek J F, Keijzer M and van Gemert M J C 1993 Modelling the effect of wavelentgth on the pulsed dye laser treatment of port wine stains *Appl. Opt.* **32** 393–8